applied sciences

MDPI

Article

A Polarization-Based Method for Maritime Image Dehazing

Rui Ma [1], Zhenduo Zhang [1,*], Shuolin Zhang [1], Zhen Wang [1] and Shuai Liu [1,2]

[1] Navigation College, Dalian Maritime University, Dalian 116026, China; marui5645@126.com (R.M.); zhang-shuolin@dlmu.edu.cn (S.Z.); 13165027618@163.com (Z.W.); lius_ciomp@163.com (S.L.)
[2] Changchun Institute of Optics, Fine Mechanics and Physics, Chinese Academy of Sciences, Dong Nanhu Road 3888, Changchun 130033, China
* Correspondence: zhangzhenduo@dlmu.edu.cn

Abstract: The accurate identification of target imagery in the presence of sea fog is essential for the precise detection and comprehension of targets situated at sea. To overcome the issues encountered when applying traditional polarimetric dehazing methods to sea fog imagery, this paper proposes an improved polarimetric dehazing method. Initially, the methodology employs quartile-based selection on polarization difference images to ascertain atmospheric light at an infinite distance. Subsequently, the study describes a segmentation approach for sea–sky background images based on the degree of polarization. The results show that the image information entropy of the segmentation process improves by more than 6% compared to that of alternative methodologies, and the local contrast of the image is increased by more than 30% compared to that of the original foggy image. These outcomes confirm the effectiveness of the proposed dehazing methodology in addressing the challenges associated with sea fog imagery.

Keywords: polarimetric imaging; image dehazing; image segmentation; sea fog

1. Introduction

Sea fog is commonly formed when warm and moist air interacts with cold sea surfaces, with its presence closely tied to the marine ecosystem [1]. The process of sea fog formation involves a high concentration of water vapor near the sea surface, causing disruptions in the behavior of electromagnetic waves at different wavelengths [2]. This can result in issues such as reduced contrast, color distortion, and blurred image details in sensor-captured images. According to the framework for view quality proposed by Ko [3], sea fog images suffer from low view clarity due to the fog and low view access due to the wide depth of field. This reduces the safety of navigation for ships in foggy conditions, leading to numerous collision accidents. Besides, the impact of sea fog extends to various maritime activities like maritime scene monitoring, shipping trade, fishing, and naval operations. Therefore, researching methods to remove sea fog is of paramount practical significance for enhancing the safety of navigation for ships and other maritime activities in foggy conditions.

To address the challenges posed by fog, researchers have proposed different dehazing methods, i.e., the dark channel prior method [4], polarimetric dehazing techniques [5–7], and deep learning-based dehazing approaches [8–10], aimed at improving production and daily activities. Polarimetric dehazing methods, which are utilized to mitigate haze effects in images, exploit differences in polarization between light scattered by the air light and directly transmitted light passing through fog particles. By employing the physical model of atmospheric scattering, these methods can differentiate between the two types of light, thereby restoring image details and effectively reducing haze. The development of detection technology has enabled the creation of polarized cameras, which have greatly improved the process of data collection. Polarimetric dehazing techniques are well-regarded for

check for updates

Citation: Ma, R.; Zhang, Z.; Zhang, S.; Wang, Z.; Liu, S. A Polarization-Based Method for Maritime Image Dehazing. *Appl. Sci.* **2024**, *14*, 4234. https://doi.org/10.3390/app14104234

Academic Editor: Atsushi Mase

Received: 18 April 2024
Revised: 13 May 2024
Accepted: 14 May 2024
Published: 16 May 2024

their minimal equipment requirements, adaptability, consistent dehazing results, and cost-effectiveness [11]. Schechner et al. [7] proposed the classic polarized-difference dehazing method, which involves capturing "brightest" and "darkest" intensity images by rotating a linear polarizer in front of the camera lens. By combining their assumptions with physical models, the researchers achieve haze-free image restoration. Liang et al. [5] suggested using Stokes vectors to calculate the angle of polarization (AOP) of scattered light and deriving the air light from this angle to generate a clear, haze-free image using a physical model. By estimating the angle of polarization for the air light, noise in the image is effectively reduced, enhancing the dehazing capability. Building on this work, Liang et al. [12–14] incorporated filtering methods to explore air light denoising, yielding positive results.

In the context of estimating the atmospheric light intensity at infinity (referred to as A_∞), various methodologies have been proposed in the literature. Shwartz et al. [15,16] have suggested an approach that involves identifying two points in an image with identical pixel values under clear weather conditions, but this method faces challenges in maritime environments where targets are often small. Liang et al. [17] introduced a technique to estimate A_∞, even in the absence of sky background conditions, by transforming formulas, although this method requires complex computations and may not be practical for sea fog images with extensive sky coverage. Some strategies incorporate the dark channel prior principle for A_∞ detection [6,18], but in maritime settings, the presence of large sky regions can lead to high pixel values across all channels, reducing the effectiveness of this principle [19,20]. Additionally, conventional polarimetric dehazing techniques may cause sea regions to appear black in dehazed images when dealing with objects that act as specular reflectors, resulting in an overestimation of the air light [21,22]. Namer [21] proposed a correction method to address this issue, suggesting the linear interpolation of air light near specular objects and using the adjusted air light for these objects. Liang [13] presented an alternative method for handling specular objects with small areas and high A_p, representing the polarized radiance of the air light, by setting a threshold based on the average A_p value and adjusting values exceeding this threshold to a slightly lower fixed value. While these approaches are suitable for scenarios where specular objects are a minor part of the image, their utility may be constrained in marine settings.

The majority of the polarimetric dehazing techniques previously discussed have been developed to reduce fog in terrestrial settings, with only a few methods focusing on sea fog. To address the limitations of the existing approaches in identifying A_∞ in sea fog environments, a new method tailored specifically for sea scenes is proposed. Considering the characteristics of marine imagery and the appearance of dark patches in maritime areas after conventional polarimetric dehazing, an improved polarimetric dehazing technique based on polarimetric segmentation is suggested. We conducted comparative experiments with existing methods on sea fog images containing ships and distant coastal scenes. The results show that the image information entropy of the segmentation process improves by more than 6% compared to that of alternative methodologies, and the local contrast of the image is increased by more than 30% compared to that of the original foggy image.

2. Related Work

2.1. The Physical Model of Atmospheric Scattering

In situations characterized by foggy weather conditions, natural light undergoes scattering and absorption by fog droplets, resulting in a decrease in the amount of energy reaching the detector and subsequently causing image blurring. McCartney [23] proposed a physical model of atmospheric scattering that has been widely employed in dehazing algorithms. The equation that embodies the physical model of atmospheric scattering is expressed as follows:

$$I = D + A = Lt + A_\infty(1 - t) \quad (1)$$

In the Equation (1), I represents the foggy image captured by the detector; D indicates the direct light; A represents the air light; A_∞ represents the air light from infinity; t represents the transmittance map of the atmosphere; $t(z) = e^{-\beta z}$; β represents the extinction

coefficient of the scattering medium; z represents the transmission distance. The equation is modified as follows to obtain the clear image L:

$$L = \frac{I - A}{1 - A/A_\infty} \tag{2}$$

2.2. Polarimetric Dehazing Method Based on Stokes Vector

The Stokes vector is utilized to characterize the polarization properties of the light that has been scattered. Polarimetric dehazing techniques, as referenced in prior research [14], rely on the Stokes vector to acquire four distinct images (I(0), I(45), I(90), and I(135)) corresponding to different polarization orientations (0°, 45°, 90°, 135°), and subsequently compute the Stokes vector according to the following formulation:

$$\begin{aligned} S_0 &= [I(0) + I(45) + I(90) + I(135)]/2 \\ S_1 &= [I(0) - I(90)] \\ S_2 &= [I(45) - I(135)] \end{aligned} \tag{3}$$

In Equation (3), S_0 represents the total intensity, S_1 represents the intensity difference between the vertical and horizontal polarized components, and S_2 represents the intensity difference between the 45° and 135° polarized components with respect to the x axis. The AOP is derived from S_1 and S_2, which contain less direct light. Therefore, estimating the air light using the AOP can effectively suppress the influence of direct light. Subsequently, within the selected sky region in the image, θ is calculated, and the most frequently occurring θ is chosen as θ_A for the sky region.

$$\theta = \frac{1}{2}\arctan\frac{S_2}{S_1} \tag{4}$$

Then, the degree of polarization p is computed, and the maximum p value within the region where θ equals θ_A is selected as the degree of polarization of the air light, denoted as p_A. Particularly, when the denominator equals 0 (i.e., $\theta = k\pi \pm \frac{\pi}{4}$), $\theta = (1 \pm 0.001) \cdot \theta_A$. Afterwards, the air light A is obtained as follows:

$$p = \frac{S_1}{S_0(\cos^2\theta_A - \sin^2\theta_A)} \tag{5}$$

$$A = \frac{A_p}{p_A} = \frac{I(0) - S_0(1-p)/2}{p_A \cdot \cos^2\theta_A} = \frac{I(90) - S_0(1-p)/2}{p_A \cdot \sin^2\theta_A} \tag{6}$$

In general, p_A is usually low. The noise within the air light A, as calculated directly from Equation (6), may be considerably increased. To mitigate the noise within A, a Gaussian low-pass filter is employed for noise reduction, as suggested in prior research [13].

$$A' = A * \frac{1}{2\pi\sigma^2}\exp[-\frac{(a-a_0)^2 + (b-b_0)^2}{2\sigma^2}] \tag{7}$$

In Equation (7), the Gaussian kernel is centered at coordinates (a_0,b_0), with *(a, b)* representing the image coordinates. The parameter σ is defined in this research as 0.1% of the total image area. Typically, dehazing methods assume a constant value for the extinction coefficient β, which may lead to discrepancies between the estimated transmittance (t) and the actual values. To address this issue, a bias coefficient ε_1 is introduced to calibrate A_∞ and improve the accuracy of the estimated transmittance, t. The optimal bias coefficient selection can be achieved by employing an evaluation function [14]. The final dehazed image can be obtained using Equation (8).

$$L = \frac{I - A'}{1 - A'/\varepsilon_1 A_\infty} \tag{8}$$

3. Experiments and Proposed Method

Images acquired over the sea often show large sky areas and noticeable polarization in the water. Traditional polarimetric dehazing methods face difficulties in achieving satisfactory results in maritime environments because of challenges in estimating infinite atmospheric light and the presence of dark areas in the haze-free image above the sea surface. To tackle these challenges, this paper introduces the following approaches.

3.1. Experimental Environment

In this research, a polarimetric camera was utilized to capture images at a coastal site under foggy weather conditions to gather the necessary experimental data and evaluate the dehazing effects of the proposed method. The weather during the shooting is cloudy, with high humidity. The camera, with a resolution of 2448 × 2048 pixels, employs a 2 × 2 pattern on its sensor to capture polarized image information for the directions of 0°, 45°, 90°, and 135°. Through image analysis, these polarized images are separated into four distinct images (I(0), I(45), I(90), I(135)), each with a resolution of 1224 × 1024. The camera was mounted on a stable platform and secured using a tripod and gimbal to ensure high-quality image acquisition. The experimental setup is illustrated in Figure 1, where Figure 1a shows a model OR-250CNC-P polarimetric camera; Figure 1b shows the lens, which has a diameter of 50 mm and a relative aperture of 1:2.8; Figure 1c depicts the combination of the camera and the lens; and Figure 1d illustrates the imaging page of the camera. The arrangement of pixels in the polarized detector is shown in Figure 2. Through image analysis, four polarimetric images can be decomposed, as shown in Figure 3.

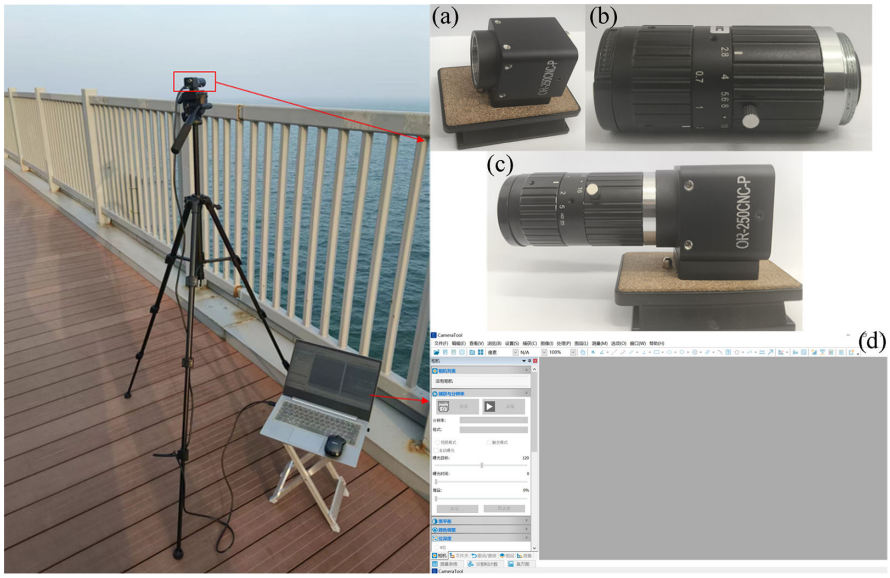

Figure 1. Experimental setup. (**a**) Polarimetric camera; (**b**) the lens; (**c**) camera and lens combination; (**d**) camera imaging page.

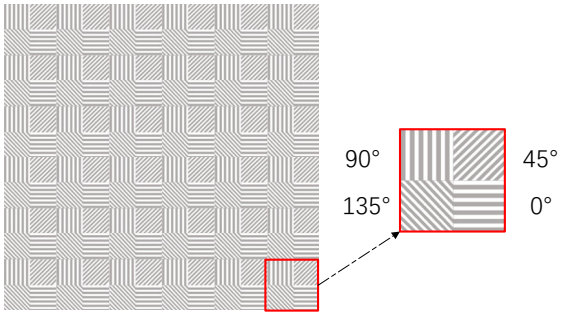

Figure 2. Distribution of the polarization detector's pixels.

Figure 3. I(0), I(45), I(90), I(135) (from left to right).

3.2. Estimation of A_∞

The identification of A_∞ plays a crucial role in the dehazing procedure. $I_\perp$ and $I_\parallel$ represent the pictures with the "brightest" and "darkest" images obtained by rotating a polarizer in front of a camera, respectively. These images depict the maximum and minimum radiance levels affected by the air light. The polarization difference image is calculated as the discrepancy between these two images. $I_\perp$ and $I_\parallel$ can also be computed using Stokes vector operations, as follows:

$$I_\perp = \frac{S_0 \cdot (1+p)}{2} \tag{9}$$

$$I_\parallel = \frac{S_0 \cdot (1-p)}{2} \tag{10}$$

$$\Delta I = I_\perp - I_\parallel \tag{11}$$

where p represents the degree of polarization, directly indicated by the Stokes vector.

$$p = \frac{\sqrt{S_1^2 + S_2^2}}{S_0} \tag{12}$$

In the context of the polarization difference image, areas beyond the sky that contain a higher density of object targets display a greater discrepancy in comparison to regions of the sky with fewer object targets. This characteristic can aid in refining the search scope for the celestial area. The variance of an image is an indicator of the level of local detail variation present in the grayscale values of the image. To achieve a precise A_∞ value, a quadrant division method is employed for the polarization difference image. This involves using a variance evaluation function to divide the image into four equal parts, with the segment expressing the lowest variance selected for further quadrant division. From the previous description, it is evident that a smaller variance typically indicates more stable pixel values in that region, suggesting fewer variations. This aligns well with the characteristics of sky regions. Hence, here we opt for the lowest variance. This process is repeated until the segmented regions are smaller than a predetermined threshold area, which has been determined through multiple experiments to be one-eighth of the size of the polarization difference image. Once the final segmented regions are identified in the polarization difference image, the corresponding regions in the S_0 image are chosen as potential regions for A_∞. The highest pixel value within each region is then designated as the A_∞ value. This methodology is illustrated in Figure 4, where Figure 4e demonstrates the process of locating A_∞ on the polarization difference image, with the white areas representing potential regions for A_∞. Subsequently, as shown in Figure 4f, the maximum pixel value is extracted from the red region and assigned as the A_∞ value.

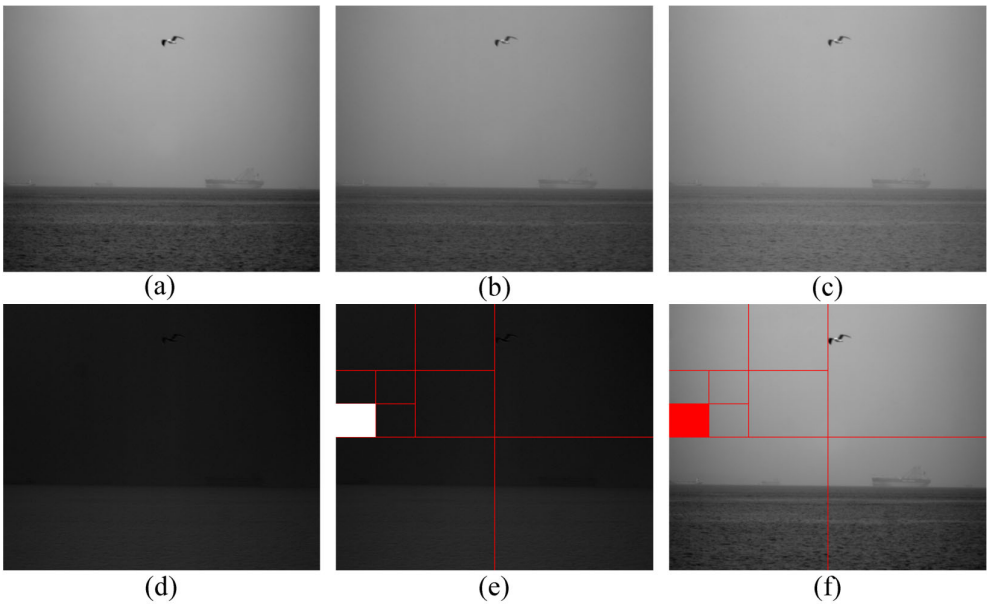

Figure 4. The process of estimating A_∞. (**a**) S_0 image; (**b**) $I_{\|}$ image; (**c**) $I_{\perp}$ image; (**d**) ΔI image; (**e**) search A_∞ on image ΔI; (**f**) operations corresponding to the S_0 image.

3.3. Separate Seawater Area

The polarimetric dehazing model operates under the assumption that direct light lacks polarization characteristics. However, research has shown that seawater exhibits significant polarization phenomena [24,25]. In fact, when objects with specular surfaces, such as glass or water, are illuminated, the direct light becomes polarized [21,26,27]. When objects with specular surfaces, such as glass or water, are illuminated, the direct light becomes polarized. This effect is particularly prominent in maritime environments, where vast bodies of water are closer to the detector than the target objects. Consequently, the polarized component of the air light in these aquatic regions is notably diminished compared to that of direct light. The presence of a large A_P in water regions, as denoted by Equation (6), results in an overestimation of parameter A, leading to the formation of dark patches in the dehazed image. Figure 5 illustrates the impact of utilizing the aforementioned polarimetric dehazing model in Section 2.2. To address this issue, a methodology is proposed for segmenting the sea surface and mitigating the influence of air light in aquatic areas. The initial step involves segmenting the seawater area, followed by the introduction of a bias coefficient ε_2 to regulate A in Equation (16). The detailed operations are described in the following paragraphs.

Figure 5. The dehazing image obtained without using the segmentation seawater method.

The technique of image segmentation through thresholding involves the categorization of pixels into separate classes based on a predefined grayscale threshold. Pixels with grayscale values falling within a specific range are grouped together. Improved segmentation results in a more pronounced differentiation in characteristics among the segmented

components. The Otsu algorithm [28], a well-known method for thresholding segmentation, is widely utilized due to its reliability. Also known as the maximum between-class variance method, the Otsu algorithm divides an image into background and target segments by examining grayscale properties. A higher between-class variance indicates greater distinctions between the two segments and a lower likelihood of misclassification. The calculation process of between-class variance can be summarized by the following formulas:

$$\mu_h = R_1 \times \mu_1 + R_2 \times \mu_2 \tag{13}$$

$$\sigma_1^2 = R_1(\mu_1 - \mu_h)^2 + R_2(\mu_2 - \mu_h)^2 = R_1 R_2(\mu_1 - \mu_2)^2 \tag{14}$$

$$\sigma_1^2(k^*) = \max_{0 \le k < M} \sigma_1^2(k) \tag{15}$$

where it is assumed that the image has M grayscale levels, with k as the classification threshold, and the total average grayscale value of the image is μ_h. The background portion consists of pixels with grayscale values ranging from 0 to k, with the proportion of these pixels to the total number of pixels denoted as R_1, and their average grayscale value as μ_1. The target portion consists of pixels with grayscale values ranging from k to $M - 1$, with the proportion of these pixels to the total number of pixels denoted as R_2, and their average grayscale value as μ_2. Substituting Equation (13) into Equation (14), we obtain the between-class variance σ_1^2. When the absolute difference between the average grayscale values of the background and target in Equation (14) is maximal, the between-class variance is maximal. As shown in Equation (15), the obtained classification threshold k is regarded as the optimal threshold k^*, representing the best segmentation result. By iterating over the values of k in the range from 0 to $M - 1$, the optimal threshold value k^* can be obtained.

The degree of polarization can indicate specific physical properties of objects, with objects composed of different materials exhibiting varying degrees of polarization. As depicted in Figure 6b, there is a significant disparity in polarization levels between the sea surface and the non-sea region in the foggy sea scene. Consequently, the decision was made to utilize the Otsu algorithm on the degree of polarization image to segment the seawater area. Subsequent to this, morphological processing techniques were employed on the segmented image. Here, we utilize the morphological closure operation to reduce gaps and refine the boundaries of the initial segmented binary image [29]. Through such processing, the seawater area will be identified more accurately. The results of the processing are presented in Figure 6, with Figure 6c showing the segmented binary image, where the sea areas are highlighted in white.

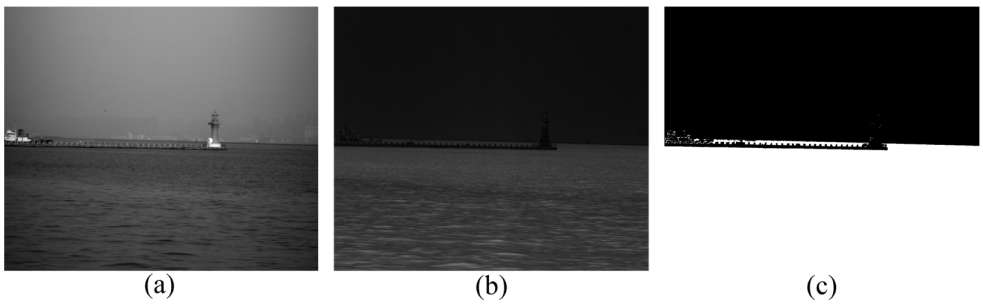

Figure 6. The process of seawater region segmentation. (**a**) S_0 image; (**b**) the degree of polarization image; (**c**) the segmentation binary image.

Due to the overestimation of air light in the sea surface region, after segmentation, we adjust the A_{sea} to an appropriate value using a bias coefficient $\varepsilon_2(\varepsilon_2 > 1)$. According to the citation provided in reference [19], the entropy function has the capability to autonomously ascertain the most suitable bias coefficient ε_2. The entropy function is defined in Equation (18), with p_k denoting the relative frequency of gray level k. Through the manipulation of ε_2 values and the subsequent creation of a series of dehazed images, the

entropy function is computed for each image. The dehazed image exhibiting the maximum entropy value is ultimately selected as the optimal dehazed image, as follows:

$$p_{A'} = p_A \cdot \varepsilon_2 \tag{16}$$

$$A_{sea} = \frac{A_p}{p_{A'}} = \frac{I(0) - S_0(1-p)/2}{p_{A'} \cdot \cos^2 \theta_A} = \frac{I(90) - S_0(1-p)/2}{p_{A'} \cdot \sin^2 \theta_A} \tag{17}$$

$$E = -\sum_k p_k \log_2 p_k \tag{18}$$

By replacing p_A with $p_{A'}$ in Equation (6), the value of A_{sea} is effectively reduced. Subsequently, a Gaussian low-pass filter is applied to A_{sea}. Finally, based on Equation (19), we obtain the haze-free sea surface region, denoted as L_{sea}. The whole workflow is shown in Figure 7.

$$L_{sea} = \frac{I - A_{sea}}{1 - A_{sea}/A_\infty} \tag{19}$$

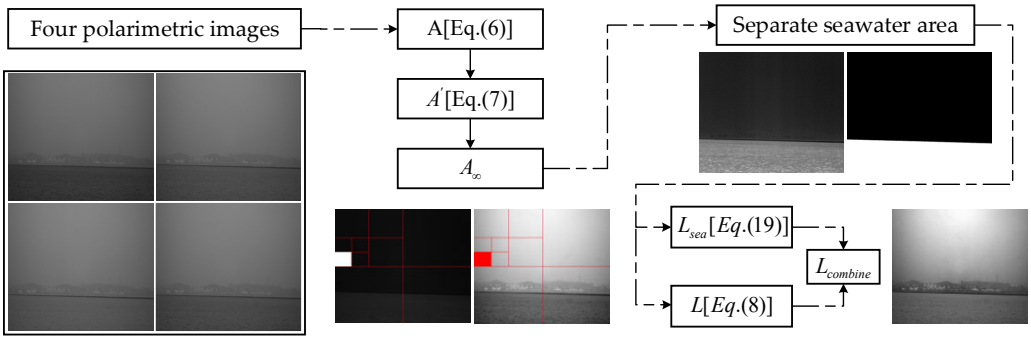

Figure 7. The workflow of the proposed method.

4. Results and Discussion

This paper compared the proposed approach with established image dehazing methods such as DCP [4], Retinex [30], and BCCR [31]. The results of the comparative analysis are presented in Figure 8, showcasing the outcomes of the different methods. The experiments were conducted on an Intel(R) Core(TM) i5 CPU (Intel, Santa Clara, CA, USA) operating at 3.2 GHz with 8 GB of RAM, and the implementation was carried out using the Python (Python 3.12. 0a1) programming language.

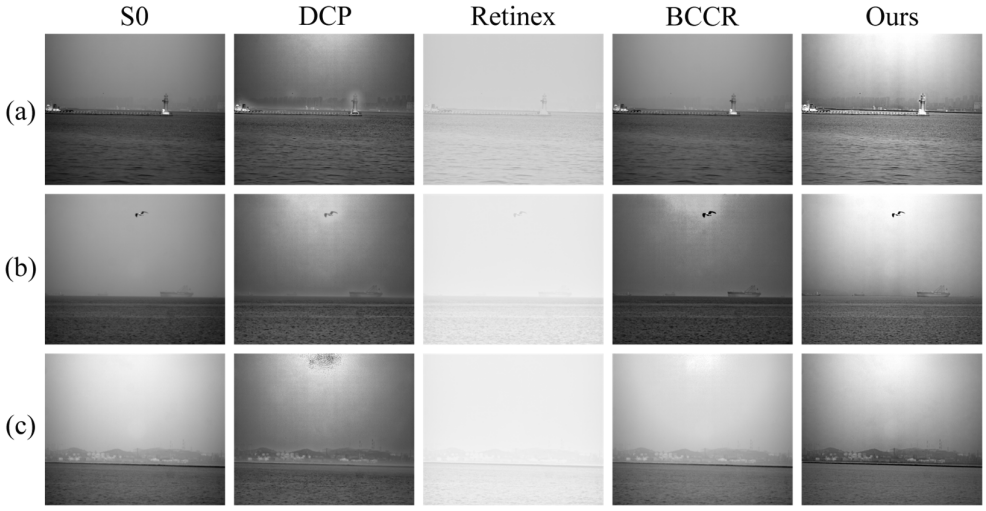

Figure 8. Comparison of results from different methods. (**a**,**b**) show images of island buildings with fog; (**c**) shows an image of ships in sea fog.

4.1. Subjective Evaluation

As shown in Figure 8, the DCP method shows improved recovery of distant structures, such as the buildings in Figure 8a and the chimney in Figure 8c. However, it exhibits significant haloing and gray distortion, especially around the boundary between the sea and the sky and near the lighthouse. Gray distortion is noticeable in the sky region of Figure 8c and the hull of the ship in Figure 8a. The Retinex method results in overly bright images, leading to reduced contrast. While the BCCR method effectively removes haze from nearby objects, its performance on distant objects is worse, with residual haze present, as seen in the distant boat in Figure 8b and the distant buildings in Figure 8a.

In Figures 9 and 10, specific regions from Figure 8a,c were selected for magnification processing to examine detailed local information. A comparative evaluation was conducted between the established DCP and BCCR methods and the newly proposed method, with the new method exhibiting effectiveness, as shown in Figure 8. In region a-1, the DCP method displays prominent halo effects near the lighthouse, affecting the retrieval of background structure details. The BCCR method shows limited success in recovering distant buildings. Conversely, our approach effectively restores details in remote buildings, with appropriate luminance levels. In region a-2, where buildings are barely distinguishable, the DCP method can partially restore some details, but halos produced by the ship obscure certain details and reduce image brightness. While the BCCR method can enhance image brightness, its ability to recover details is restricted. Our method reveals distant windows and building edges, with suitable brightness, effectively restoring building details. In regions b-3 and b-4, the DCP method excels in detail recovery but generates halos along mountain edges. The BCCR method enhances image brightness but lacks detail recovery. In contrast, our method successfully achieves robust detail recovery without inducing halos, and notably, it provides a contrast that surpasses that of the aforementioned methods.

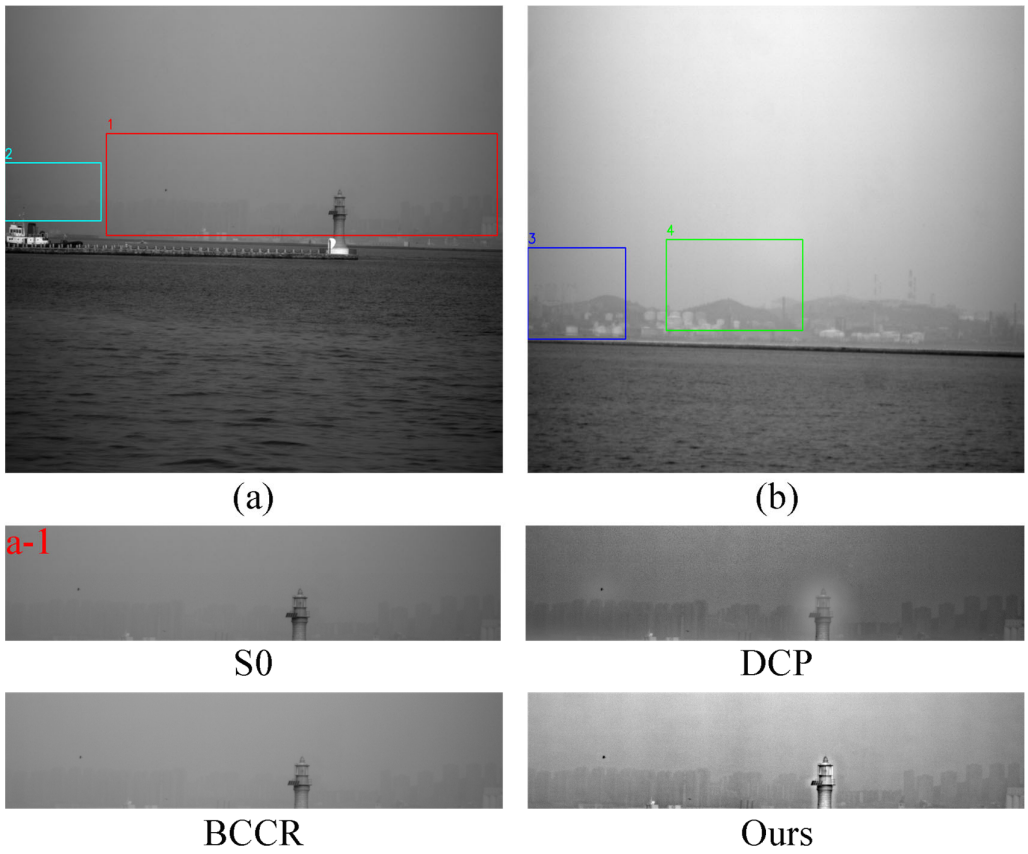

Figure 9. S_0 images and zoom images from region a-1 (**a**,**b**).

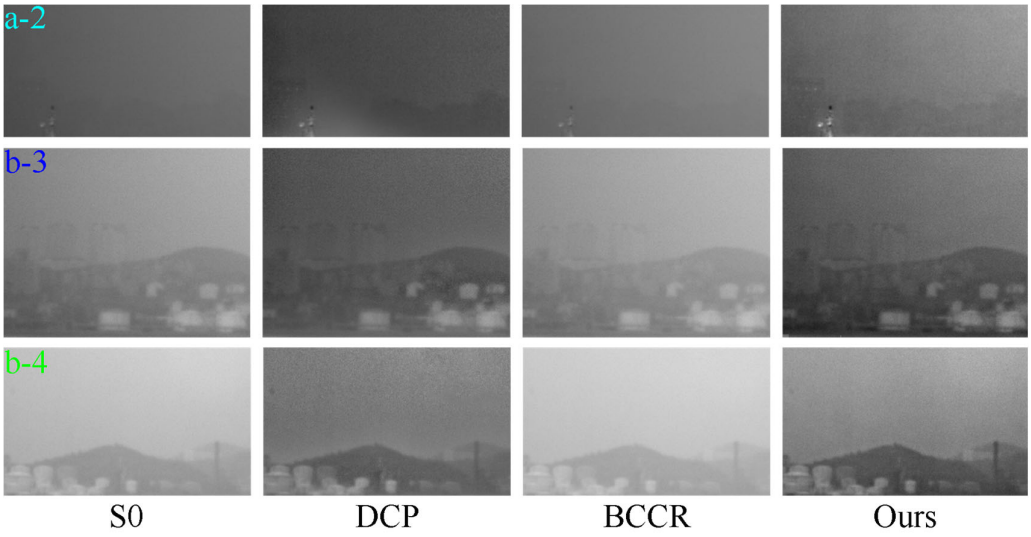

Figure 10. Zoom images from regions a-2, b-3, and b-4.

Both the DCP and BCCR methods utilize the dark channel prior theory, which requires at least one channel of the three to have pixel values close to zero. However, this theory may not be applicable to sea fog images with large sky regions, leading to the inaccurate estimation of A_∞. Additionally, in obtaining the dark channel map, DCP disrupts the edges of the image transitions, resulting in inaccurate estimation of the transmittance map of the atmosphere tending to include blocky and halo effects. The Retinex method, due to its adoption of grayscale assumptions, leads to low-contrast images. Our method utilizes an abundance of polarization information (the angle of polarization, the degree of polarization, polarization difference image), which is superior in information dimensionality compared to other methods. Moreover, our method is specifically designed for the distinctive scenario of sea fog. By using polarization difference information, we can effectively estimate a suitable A_∞. The combined use of the angle of polarization and the degree of polarization can better estimate the transmission map of the atmosphere.

The gray level histogram functions as a statistical representation of the distribution of pixel intensities in an image, offering a visual portrayal of the improvement in a foggy image. As shown in Figure 11, gray level histograms were computed for different methods applied to the images shown in Figure 8b. A wider histogram indicates higher image quality and greater detail. The gray level histogram of our proposed approach exhibits superior efficacy when compared to alternative methods.

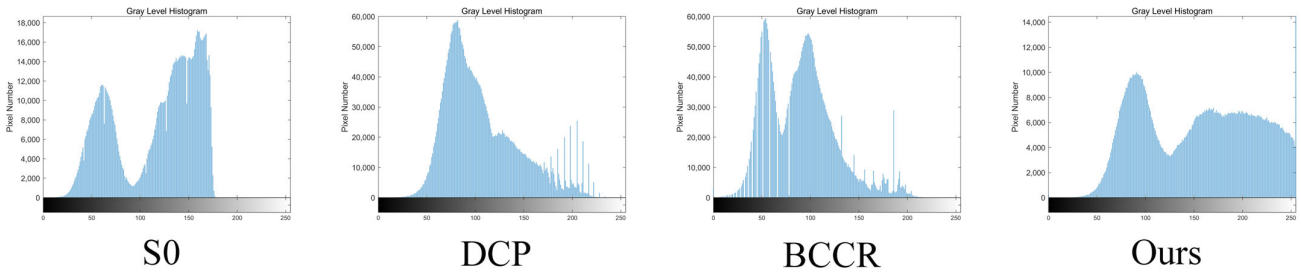

Figure 11. The gray level histograms of different methods in Figure 8b.

4.2. Objective Evaluation

In order to objectively assess the effectiveness of our proposed dehazing method, a quantitative analysis was conducted utilizing four image evaluation metrics: image entropy, average gradient, image standard deviation, and image contrast. Image entropy measures the amount of information present in an image, with higher entropy values indicating a

greater information content and improved image quality. The average gradient reflects the rate at which contrast changes occur in small image elements, thereby indicating the clarity of the image, to some extent. The standard deviation reflects the degree that the gray value deviates from the average value. The better image has a larger standard deviation. The evaluation results of the dehazed images obtained through different methodologies are presented in Table 1. It is evident from the table that our proposed method exhibits superior image entropy and standard deviation values compared to the other methods, indicating its ability to preserve more information and enhance image edge clarity. Although our method shows slightly lower performance for the average gradient compared to the DCP method for Figure 8b,c, the difference is minimal. Table 2 presents the local contrast results of the images, showing that our method significantly improves image contrast compared to that of the original foggy images. For each measure, we use bold type to indicate the highest value in Tables 1 and 2. Additionally, Table 3 provides the computation of time costs for various methods. Compared with other algorithms, the computational efficiency of the method proposed in this paper is not perfect, requiring further improvement in the future.

Table 1. Evaluations of methods.

	Method	Entropy	Average Gradient	Standard Deviation
Image (1)	DCP	15.4769	4.5305	30.5919
	Retinex	7.6614	2.4876	6.2811
	BCCR	15.7931	3.2304	36.3609
	Proposed	**17.3816**	**4.5755**	**45.7123**
Image (2)	DCP	16.5102	**4.5126**	38.9366
	Retinex	6.9300	1.8675	5.1372
	BCCR	16.0234	4.5028	35.4737
	Proposed	**18.1069**	4.4429	**58.2767**
Image (3)	DCP	16.8367	**4.5385**	42.4886
	Retinex	6.7863	1.9913	4.9608
	BCCR	16.7242	3.8062	48.8653
	Proposed	**17.9113**	4.3091	**53.5727**

Table 2. Image contrast of different methods.

	S0	DCP	BCCR	Proposed
a-1	0.7430	1.0000	0.6602	**1.0000**
a-2	0.3743	0.6354	0.3116	**0.8559**
b-3	0.3916	0.4751	0.3242	**0.6778**
b-4	0.2465	0.4188	0.1957	**0.5854**

Table 3. Computational cost of different methods.

	DCP	Retinex	BCCR	Proposed
Run time (sec)	**0.4370**	11.8328	5.0523	10.3335

4.3. Limitations of the Proposed Method

Our approach addresses the limitations of traditional polarimetric dehazing methods for fog removal in maritime fog conditions. However, there are situations where it may exhibit insufficient segmentation of sea regions. For example, in Figure 12c, the methodology incorrectly identifies rooftops and parts of the boat as sea regions (indicated by white areas representing sea regions). This misclassification occurs when the degree of polarization of objects closely matches that of the surrounding sea and when these objects occupy a significant portion of the overall image area, leading to inaccurate segmentation. To address

this issue, we plan to introduce enhancements specifically tailored for such images. These enhancements will involve refining the degree of polarization calculations, incorporating target contour detection, and implementing other improvements.

Figure 12. Failed segmentation case. (**a**) the S_0 image; (**b**) the degree of polarization image; (**c**) the segmentation binary image.

5. Conclusions

This research study presents an improved polarimetric method that addresses the constraints of traditional polarimetric dehazing techniques in marine settings. By employing a quadrant technique alongside polarization difference images, the automated and efficient extraction of A_∞ is achieved. Additionally, segmenting the sea area based on the intensity of the polarization image aids in subsequent dehazing procedures, effectively overcoming the defect encountered by conventional polarimetric dehazing methods in marine environments. Comparative analysis with the DCP method reveals an increase in image entropy ranging from 6% to 12%, a rise in standard deviation by 26% to 49%, and an average contrast enhancement of 29%. In contrast to the BCCR method, the proposed approach demonstrates an increase in image entropy between 7% and 13%, an increase in standard deviation from 9% to 64%, and a contrast elevation of 51% to 199%. Notably, it displays significant performance improvements compared to the Retinex method. The local contrast of the images is improved by over 30% compared to that of the original foggy images. Experimental findings demonstrate the suitability of the proposed method for marine scenes, effectively leveraging polarization data for dehazing and successfully restoring image detail information. However, as described in Section 3.2, we used multiple experiments to establish the predetermined threshold area, and in the future, we plan to employ more systematic solutions, such as the Nyquist–Shannon Criterion. In addition, as discussed in Section 4.3, our method may encounter mis-segmentation in certain specific environments. We will seek to further improve this in future work.

Author Contributions: Conceptualization, Z.Z. and R.M.; methodology, R.M.; software, R.M.; validation, Z.Z. and S.L.; formal analysis, R.M.; investigation, S.Z.; resources, S.Z.; data curation, R.M. and Z.W.; writing—original draft preparation, R.M.; writing—review and editing, Z.Z., S.L. and R.M.; visualization, Z.W. and S.Z.; supervision, Z.Z.; project administration, Z.Z.; funding acquisition, Z.Z. All authors have read and agreed to the published version of the manuscript.

Funding: This research received no external funding.

Institutional Review Board Statement: Not applicable.

Informed Consent Statement: Not applicable.

Data Availability Statement: The raw data supporting the conclusions of this article will be made available by the authors on request.

Acknowledgments: We appreciate the assistance provided by Qilong Jia during the early stages of the experiment.

Conflicts of Interest: The authors declare no conflicts of interest.

References

1. Zhang, S. Recent observations and modeling study about sea fog over the Yellow Sea and East China Sea. *J. Ocean Univ. China* **2012**, *11*, 465–472. [CrossRef]
2. Kim, C.K.; Yum, S.S. Local meteorological and synoptic characteristics of fogs formed over Incheon international airport in the west coast of Korea. *Adv. Atmos. Sci.* **2010**, *27*, 761–776. [CrossRef]
3. Ko, W.H.; Kent, M.G.; Schiavon, S.; Levitt, B.; Betti, G. A window view quality assessment framework. *Leukos* **2022**, *18*, 268–293. [CrossRef]
4. He, K.; Sun, J.; Tang, X. Single image haze removal using dark channel prior. *IEEE Trans. Pattern Anal. Mach. Intell.* **2010**, *33*, 2341–2353. [PubMed]
5. Liang, J.; Ren, L.; Qu, E.; Hu, B.; Wang, Y. Method for enhancing visibility of hazy images based on polarimetric imaging. *Photonics Res.* **2014**, *2*, 38–44. [CrossRef]
6. Liu, S.; Li, Y.; Li, H.; Wang, B.; Wu, Y.; Zhang, Z. Visual Image Dehazing Using Polarimetric Atmospheric Light Estimation. *Appl. Sci.* **2023**, *13*, 10909. [CrossRef]
7. Schechner, Y.Y.; Narasimhan, S.G.; Nayar, S.K. Polarization-based vision through haze. *Appl. Opt.* **2003**, *42*, 511–525. [CrossRef] [PubMed]
8. Li, L.; Dong, Y.; Ren, W.; Pan, J.; Gao, C.; Sang, N.; Yang, M.-H. Semi-supervised image dehazing. *IEEE Trans. Image Process.* **2019**, *29*, 2766–2779. [CrossRef]
9. Liu, Z.; Lin, Y.; Cao, Y.; Hu, H.; Wei, Y.; Zhang, Z.; Lin, S.; Guo, B. Swin transformer: Hierarchical vision transformer using shifted windows. In Proceedings of the IEEE/CVF International Conference on Computer Vision, Montreal, BC, Canada, 11–17 October 2021; pp. 10012–10022.
10. Qin, X.; Wang, Z.; Bai, Y.; Xie, X.; Jia, H. FFA-Net: Feature fusion attention network for single image dehazing. In Proceedings of the AAAI Conference on Artificial Intelligence, New York, NY, USA, 7–12 February 2020; pp. 11908–11915.
11. Zhang, W.; Liang, J.; Wang, G.; Zhang, H.; Fu, S. Review of passive polarimetric dehazing methods. *Opt. Eng.* **2021**, *60*, 030901. [CrossRef]
12. Liang, J.; Ju, H.; Ren, L.; Yang, L.; Liang, R. Generalized polarimetric dehazing method based on low-pass filtering in frequency domain. *Sensors* **2020**, *20*, 1729. [CrossRef]
13. Liang, J.; Ren, L.; Liang, R. Low-pass filtering based polarimetric dehazing method for dense haze removal. *Opt. Express* **2021**, *29*, 28178–28189. [CrossRef] [PubMed]
14. Liang, J.; Ren, L.; Ju, H.; Zhang, W.; Qu, E. Polarimetric dehazing method for dense haze removal based on distribution analysis of angle of polarization. *Opt. Express* **2015**, *23*, 26146–26157. [CrossRef] [PubMed]
15. Shwartz, S.; Namer, E.; Schechner, Y.Y. Blind haze separation. In Proceedings of the 2006 IEEE Computer Society Conference on Computer Vision and Pattern Recognition (CVPR'06), New York, NY, USA, 17–22 June 2006; pp. 1984–1991.
16. Namer, E.; Shwartz, S.; Schechner, Y.Y. Skyless polarimetric calibration and visibility enhancement. *Opt. Express* **2009**, *17*, 472–493. [CrossRef] [PubMed]
17. Liang, J.; Ren, L.-Y.; Ju, H.-J.; Qu, E.-S.; Wang, Y.-L. Visibility enhancement of hazy images based on a universal polarimetric imaging method. *J. Appl. Phys.* **2014**, *116*, 173107. [CrossRef]
18. Zhang, W.; Liang, J.; Ju, H.; Ren, L.; Qu, E.; Wu, Z. Study of visibility enhancement of hazy images based on dark channel prior in polarimetric imaging. *Optik* **2017**, *130*, 123–130. [CrossRef]
19. Guo, T.; Li, N.; Zhang, C. Improved dark channel prior single image defogging. In Proceedings of the 2021 33rd Chinese Control and Decision Conference (CCDC), Kunming, China, 22–24 May 2021; pp. 7414–7419.
20. Ke, K.; Zhang, C.; Wu, M.; Sun, Y. Improved defogging algorithm for sea surface images based on dark channel prior theory. *Opt. Eng.* **2021**, *60*, 033104. [CrossRef]
21. Namer, E.; Schechner, Y.Y. Advanced visibility improvement based on polarization filtered images. In Proceedings of the Polarization Science and Remote Sensing II, San Diego, CA, USA, 31 July–4 August 2005; pp. 36–45.
22. Qu, Y.; Zou, Z. Non-sky polarization-based dehazing algorithm for non-specular objects using polarization difference and global scene feature. *Opt. Express* **2017**, *25*, 25004–25022. [CrossRef]
23. McCartney, E.J. *Optics of the Atmosphere: Scattering by Molecules and Particles*; Wiley: New York, NY, USA, 1976.
24. Talmage, D.; Curran, P. Remote sensing using partially polarized light. *Int. J. Remote Sens.* **1986**, *7*, 47–64. [CrossRef]
25. Tonizzo, A.; Ibrahim, A.; Zhou, J.; Gilerson, A.; Twardowski, M.; Gross, B.; Moshary, F.; Ahmed, S. Estimation of the polarized water leaving radiance from above water measurements. In Proceedings of the Ocean Sensing and Monitoring II, Orlando, FL, USA, 5–6 April 2010; pp. 17–26.
26. Schechner, Y.Y.; Nayar, S.K. Generalized mosaicing: Polarization panorama. *IEEE Trans. Pattern Anal. Mach. Intell.* **2005**, *27*, 631–636. [CrossRef]
27. Schechner, Y.Y.; Shamir, J.; Kiryati, N. Polarization and statistical analysis of scenes containing a semireflector. *JOSA A* **2000**, *17*, 276–284. [CrossRef]
28. Ostu, N. A threshold selection method from gray-level histograms. *IEEE Trans. SMC* **1979**, *9*, 62.
29. Najman, L.; Talbot, H. *Mathematical Morphology: From Theory to Applications*; John Wiley & Sons: Hoboken, NJ, USA, 2013.

30. Petro, A.B.; Sbert, C.; Morel, J.-M. Multiscale retinex. *Image Process. Line* **2014**, *4*, 71–88. [CrossRef]
31. Meng, G.; Wang, Y.; Duan, J.; Xiang, S.; Pan, C. Efficient image dehazing with boundary constraint and contextual regularization. In Proceedings of the IEEE International Conference on Computer Vision, Sydney, Australia, 1–8 December 2013; pp. 617–624.